# Arrangement of sensors and probability of detection for sensing sheets based on large-area electronics for reliable structural health monitoring

FINAL REPORT
January 2016

Submitted by:

Branko Glisic
Associate Professor

Princeton University
Princeton University E330 EQuad
Princeton, NJ 08544

External Project Manager
Prof. Franklin Moon
Department of Civil and Environmental Engineering
Rutgers University

In cooperation with

Rutgers, The State University of New Jersey
And
U.S. Department of Transportation Federal Highway Administration

# Disclaimer Statement

The contents of this report reflect the views of the authors, who are responsible for the facts and the accuracy of the information presented herein. This document is disseminated under the sponsorship of the Department of Transportation, University Transportation Centers Program, in the interest of information exchange. The U.S. Government assumes no liability for the contents or use thereof.

The Center for Advanced Infrastructure and Transportation (CAIT) is a National UTC Consortium led by Rutgers, The State University. Members of the consortium are the University of Delaware, Utah State University, Columbia University, New Jersey Institute of Technology, Princeton University, University of Texas at El Paso, Virginia Polytechnic Institute and University of South Florida. The Center is funded by the U.S. Department of Transportation.

| 1. Report No. | 2. Government Accession No. | 3. Recipient's Catalog No. | |
|---|---|---|---|
| CAIT-UTC-NC7 | | | |
| 4. Title and Subtitle<br>Arrangement of sensors and probability of detection for sensing sheets based on large-area electronics for reliable structural health monitoring | | 5. Report Date<br>January 2016<br>6. Performing Organization Code<br>CAIT/Princeton University | |
| TECHNICAL REPORT STANDARD TITLE PAGE<br>7. Author(s)<br>Branko Glisic, Ph.D. | | 8. Performing Organization Report No.<br>CAIT-UTC-NC7 | |
| 9. Performing Organization Name and Address<br>Princeton University<br>Princeton University E330 EQuad, Princeton, NJ 08544 | | 10. Work Unit No.<br>11. Contract or Grant No.<br>DTRT13-G-UTC28 | |
| 12. Sponsoring Agency Name and Address<br>Center for Advanced Infrastructure and Transportation<br>Rutgers, The State University of New Jersey<br>100 Brett Road<br>Piscataway, NJ 08854 | | 13. Type of Report and Period Covered<br>Final Report<br>02/01/2014 – 01/31/2016<br>14. Sponsoring Agency Code | |
| 15. Supplementary Notes<br>US Department of Transportation, Office of the Assistant Secretary for Research and Technology (OST-R)<br>1200 New Jersey Avenue, SE<br>Washington, DC 20590-0001 | | | |
| 16. Abstract<br>In a previous UTC project, a prototype of a novel multi-sensor sheet, called sensing sheet was developed. This sheet is based on technology called large-area electronics (LAE) and consists of dense arrays of sensors supporting several different electronic components (interconnects, circuits, batteries, etc.) that are patterned or laminated on a polyimide substrate. It has potential to cover large areas of structures and reliably identify the damage occurring virtually at any location within the sheet. The sensing sheet contains dense array of individual sensors, but there are some non-instrumented spaces between the sensors that are not directly sensitive to strain anomalies. In addition, individual sensors are sensitive to strain in one specific direction, while the damage (e.g., cracking of concrete and bowing of steel), can generate strain field anomalies that do not necessarily occur in the same direction. If the sensor network is not designed correctly, all these effects can potentially lead to unsuccessful damage identification. To address the above challenges, probabilistic approaches are needed to establish a sensor network within LAE based on the probability that this particular network can detect a damage of a certain size (probability of detection). Thus, the objective of this project was to create methodology for design of sensor network for LAE sensing sheets that will enable reliable identification of damage of a given size. The outcomes include (1) the methodology for determination of (a) arrangement of sensors and (b) probability of detection, and (2) practical guidelines with associated "probability of detection" diagrams for the most frequent types of damage. The project description and outcomes are presented in detail in the report. | | | |
| 17. Key Words<br>Structural health monitoring, Crack detection, Arrangement of a dense array of sensors, Strain monitoring, Probability of Detection, Large area electronics | 18. Distribution Statement | | |
| 19. Security Classification (of this report)<br>Unclassified | 20. Security Classification (of this page)<br>Unclassified | 21. No. of Pages<br>35 | 22. Price |

**Form DOT F 1700.7** (8-69)

## Acknowledgments

The large-scale tests on steel plates equipped with sensing sheets were carried out at the Carleton Laboratory in Columbia University. Steel specimens and associated accessories were provided by the University of Delaware. Sensing sheets were provided by Princeton University.

The authors would like to thank Y. Yao, S-T. E. Tung, D. Smith, Prof. N. Verma, Y. Hu, L. Huang, N. Lin, W. Rieutort-Louis, J. Sanz-Robinson, T. Liu, Prof. J. C. Sturm, and Prof. S. Wagner, all from Princeton University, for their precious advice and help in the project. Furthermore, thanks go to L. Mhamdi, A. Tabrizi, N. Ramanna, and G. Wenczel from the University of Delaware for assisting with testing and data analysis. Final thanks go to L. Li and E. Sporer from Columbia University for precious help in realization of fatigue test.

## Table of Contents



## List of Figures

**Page**

## DESCRIPTION OF THE PROBLEM

Many bridges in the country have reached their intended service life limit. Some of them do not pass current load-ratings or show deterioration such as corrosion and cracking. Monies for replacement and repair of bridges, however, are scarce. In order to keep these critical infrastructure components in operation, inspection, maintenance, and structural health monitoring (SHM) play a vital role. However, SHM is scarcely used on real structures since an efficient approach for its implementation has not been developed yet, and particular challenges represent reliability in damage identification and transformation of SHM data into an information useful for the end users (owner and managers of structures or even every-day users). Hence, to address the above challenges, a need exists for a cost-effective sensing approach that is able to incorporate dense array of sensors to maximize the chances for capturing and characterizing damage. The PI proposes direct sensing approach, where anomalies are sensed at close proximity via a dense array of sensors. Dense arrays can be realized using innovative technology - large area electronics (LAE) - which enables sensors, processor, communication devices and power harvesting to be embedded in thin plastic sheets that are then installed over large area of structure. Crucial challenge to be addressed in this research is design of dense sensing network for LAE sensing sheet and its reliability in damage identification, i.e., detection, localization, quantification and prognosis.

The LAE sensing sheet contains dense array of individual sensors, but there are some non-instrumented spaces between the sensors that are not sensitive to strain anomalies. In addition, individual sensors are sensitive to strain in one specific direction, while the damage (e.g., cracking of concrete and bowing of steel), can generate strain field anomalies that do not necessarily occur in the same direction. If the sensor network is not designed correctly, all these effects can potentially lead to unsuccessful damage identification.

To address the above challenges, probabilistic approaches are needed to establish a sensor network within LAE based on the probability that this particular network can detect a damage of a certain size (probability of detection). Thus, the objective of this project is to create methodology for design of sensor network for LAE sensing sheets that will enable reliable identification of damage of a given size. The methodology will be based on probabilistic approach and it will take into account the size of the LAE sensing sheet, size of the individual sensor, angular sensitivity of the sensor to damage, and orientation and size of the damage.

The outcomes of the project are (1) the methodology for determination of (a) arrangement of sensors and (b) probability of detection, and (2) practical guidelines with associated "probability of detection" diagrams for the most frequent types of damage.

## APPROACH

Materials fail at a point when the stress at that point exceeds the ultimate limit state, i.e. the strength at that point. Strain is a parameter directly correlated to stress, and so any change in the stress field is reflected through a change in the strain field. There is no effective means to directly monitor stress under real, on-site conditions; consequently, strain (static and/or dynamic) has emerged as an important parameter in SHM [3-5]. The first signs of damage to a

structure often have local character and occur in the form of strain-field anomalies (e.g., cracks and bowing in steel, and non-structural cracks in concrete). Thus, this research focuses on strain.

First, analytical and numerical methods (Monte Carlo simulation) are used to evaluate the overall probability that damage of a certain size can occur in the area covered by the sheet. Then, based on above probability the size and spacing of sensors can be determined such that the sensing sheet can detect the strain field anomaly with desired probability. Subsequently, the methodology is enlarged to encompass variable directional sensitivity of the individual sensor. Finally, the probability density function of damage orientation is evaluated based on analytical models used in structural analysis and design. Validation of the methodology is performed using data sets generated in previous UTC Tier I project [6].

## METHODOLOGY

An overview of the proposed tasks for this project and the time line are listed below, followed by a detailed description of each task. At the end of this section, the references for this proposal are listed.

(1) Probability of detection for sensors with uniform angular sensitivity
Task 1.1: Detailed literature review
Task 1.2: Determination of probability of detection using analytical and numerical methods

(2) Probability of detection for sensors with angular sensitivity
Task 2.1: Evaluation of angular sensitivity of full-bridge strain sensor
Task 2.2: Determination of probability of detection using analytical and numerical methods

(3) Probability of detection for strain distributions based on mechanical analytical models
Task 3.1: Exploration and development of probability density functions for concrete structures based on mechanical analytical models (theory of structures and solid mechanics)
Task 3.2: Exploration and development of probability density functions for steel structures based on mechanical analytical models (theory of structures and solid mechanics)

(4) Validation
Task 4.1: Comparison of results of Tasks 1 with numerical simulations performed using SAP or ABAQUS software )
Task 4.2: Comparison of results of Tasks 2 with numerical simulations performed using SAP or ABAQUS software )
Task 4.3 Comparison of results of Tasks 3 (i.e., of the developed methodology) with data sets from large-scale laboratory testing performed in the frame of the previous UTC Project [6]

The first task investigated theoretically and numerically how the density and concentration of

sensors (distribution within the sensing sheet) affect the probability of detection. The damage size and orientation that potentially could occur will be modeled using uniform distribution and the sensor will be assumed to have the same sensitivity to damage regardless the orientation of the damage with respect to sensor. This basic case will be validated by comparison with numerical simulations of a simply supported beam exposed to excessive load. The second task enlarges the application of the method created in Task 1 to encompass variable sensitivity of the sensor in different directions (angles of damage with respect to sensor). The validation is again performed based on numerical models. Finally, the third tasks completes the methodology as it will take into account non-uniform distribution of the damage size and orientation; the damage is more likely to occur in directions of principal stresses and thus the probability density function for the damage will be built based on analytical solutions (design and theory of structures) combined with Gaussian distribution. Validation of the methodology will be made by comparison with the data sets collected in large-scale testing of the LAE sensing sheet performed within the previous UTC project [6].

## FINDINGS

### Probability of detection for sensors with uniform angular sensitivity

The probability of detection (POD) is a metric used to quantify the reliability of inspection systems. The effectiveness of different SHM techniques can be characterized by a POD curve that relates the size of damage to the probability of (correct) detection. For example, the value of the POD for a crack of size *L* is defined to be the mean probability of detection of all cracks of size *L*. The POD curve may also be interpreted as the percentage of all possible defects of a given size that would be detected using a specific SHM method on a structure.

*Summary of detailed literature review*

Analytical calculations of probability of crack detection are complex due to the fact that it is practically impossible to estimate the exact location and dimensions of a crack before it has occurred. Additionally, most SHM techniques are imperfect and susceptible to detection errors inherent to monitoring system itself. Consequently, the POD curves are frequently generated in a statistical manner. However, several researchers have developed analytical probabilistic models as well. Achenbach and Kulkarni's work [7] focused on the detection of surface-breaking fatigue cracks in metals. Figure 1 shows three POD curves that were considered in their analysis, with curve "A" as the best inspection technique (higher PODs for smaller crack lengths) and curve "C" as the worst. Achenbach and Kulkarni researched unspecific POD curves and assumed that they were known for a general inspection technique.

Cohen et al. [8] researched probabilistically the growth and detection of cracks under cyclic loading, in which they considered the same general POD curves shown in Figure 1. The numerical results of both studies showed that using a SHM technique with a steeper POD curve significantly reduces the probability of an undetected crack, which emphasizes the importance of sensor arrangement.

Fujimoto et al. [9] estimated the POD for visual inspections. Most POD curves are only characterized in terms of crack length, which is generally considered the most important physical parameter. However, other factors such as location, orientation, crack width, and surface conditions can also affect the probability of crack detection in visual inspections.

Fujimoto et al. incorporated the influence of these other factors by using total probability to evaluate the POD for a crack of length $L$. They denote the probability of existence of cracks belonging to class $i$ as $q_i$ and the detection of probability of class $i$ cracks as $p_i(L)$. Therefore, the detection probability for all classes of cracks of length $L$ can be expressed as:

$$POD(L) = \sum_{1}^{n} q_i p_i(L) \tag{1}$$

where $\sum_{i=1}^{n} q_i = 1.0$.

The probabilities $q_i$ and $p_i$ were estimated from the results of many field inspections.

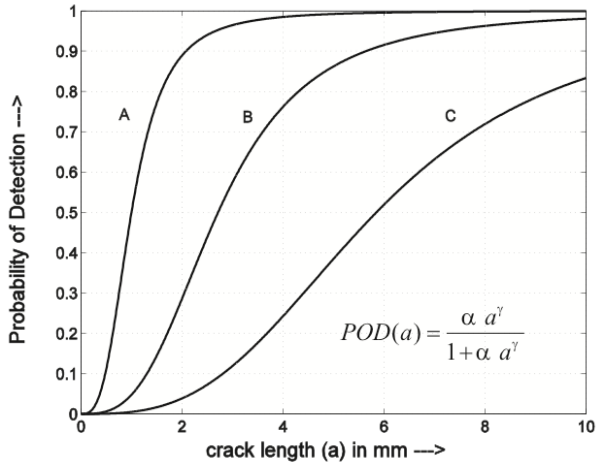


Figure 1. POD curves used in Achenbach and Kulkarni's work [7].

Different probabilistic POD curves have been developed for other SHM methods including the vibrothermography technique, ultrasonic waveforms sensing, and the eddy-current based method. However, all these techniques deal with truly distributed direct sensing, as opposed to sensing sheets that consist of dense arrays of individual (or unit) sensors. For that reason they are not presented in this report. Hence, the work presented here uses the fundamentals of POD that were developed in above presented summary of literature review.

*Determination of probability of detection using analytical and numerical methods*

This section practically addresses the question "what is the most efficient arrangement of the unit sensors in the sensing sheet, so that the arrangement has the best performance in damage detection". Hence, we studied what is the sensor arrangement that provides the most efficient probability of detection (POD) for a given size of sensing sheet area, and given number and size of unit sensors. A POD is characterized by two properties: the first is the $POD_{max}$ and the second is the crack length at which the $POD_{max}$ is achieved (critical crack length $L_{cr}$.). Higher $POD_{max}$ provides higher probability of crack detection in general, while shorter critical crack length (a steeper slope before the POD reaches the plateau) indicates higher probability of detecting minute cracks. Thus the $POD_{max}$ and $L_{cr}$. are selected as the indicators of effectiveness of POD.

The Monte Carlo simulations were performed with order of 100,000 times to generate numerical results. For the purpose of comparison of various scenarios, the surface area was identical in each scenario. In this task, the sensor is assumed to have the same sensitivity to crack, regardless the angle of the crack with respect to sensor.

Single-sensor scenarios

Various single-sensor scenarios were studied first and then the study was expanded to various multi-sensor scenarios. Three typical single sensor scenarios were evaluated, as shown in Figure 2. Case 1 analyzes the POD of a single sensor located in the center (symmetric in both horizontal and vertical directions) of a 40 mm by 40 mm surface area, with all other dimensions as shown in the left image of Figure 2. In Case 2, the sensor is shifted to the left (symmetric in only one direction), with all the dimensions as shown in the middle image of Figure 2. Finally, Case 3 analyzes the sensor positioned in the corner of the surface area (sensing sheet), and the dimensions are shown in the right image of Figure 2.

The POD vs. crack length is shown for all three cases in Figure 3. For small crack lengths (below 9 mm in the observed scenarios) all three POD graphs are identical. However, as the crack length increases, the POD graphs separate, Case 1 having the highest $POD_{max}$ and Case 3 the lowest $POD_{max}$. In addition, the critical crack length for the Case 1 is 40 mm while for two other cases the critical crack length is larger.

In summary, Case 1 is the most effective arrangement for single-sensor scenario, which indicates that we should locate the sensor symmetrically for both horizontal and vertical directions (symmetric center in this case) in order to get the maximum probability of crack detection. Case 2 is less effective and Case 3 is the least effective arrangement, and thus they should be avoided.

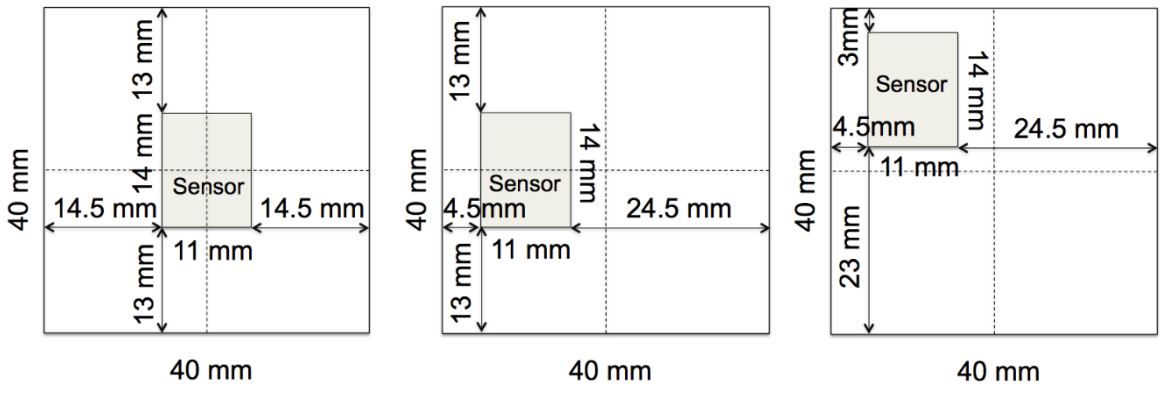


Figure 2. Left: sensor in the center of the sensing sheet (Case 1); Middle: sensor shift to the left of the sensing sheet (Case 2); Right: sensor in the corner of the sensing sheet (Case 3).

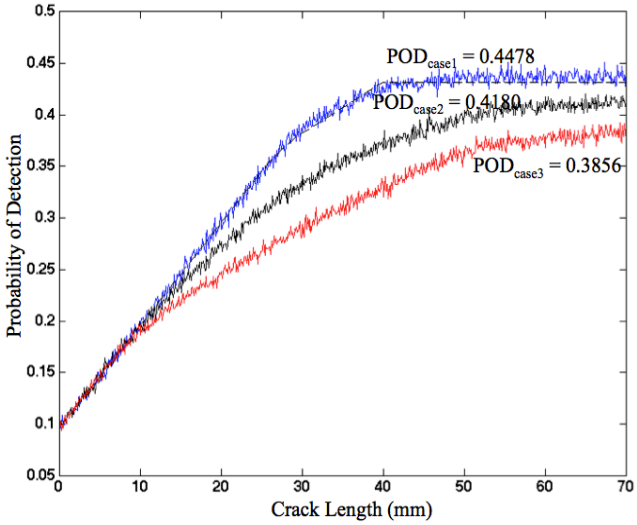


Figure 3. MCS solutions for POD of single-sensor scenarios Case 1 (the highest graph, with analytical solution in dashed line), Case 2 and Case 3 (the lowest graph).

Multi- sensor scenarios

Based on the discussion presented in previous subsection, the principle of horizontal and vertical symmetry can be extended to multiple sensor arrangements. This establishes the principle of symmetry for multiple sensor arrangements.

However, establishing principle of symmetry is not sufficient, as there is infinite number of cases that could be considered. Thus, the relative mutual positions of sensors, i.e. the horizontal and vertical distances between any two adjacent sensors should also be taken into account. Similar to the analysis presented above, it is not immediately clear whether the most effective arrangement of sensors would have uniform (equidistant) distribution within the observed area (i.e., the mutual distances between the sensors, as well as the distance between the outer sensors and the boundaries of the observed surface area should be the same), or the distance between the sensors should be two times larger than the distance to the boundaries. To identify more efficient arrangement, four-sensor scenarios (Cases 4 and 5) and nine-sensor scenarios (Cases 6 and 7) were modeled by MCS. The geometries of these two studies are presented in Figures 4 and 5 respectively.

In Case 4 (Figure 4, left), four sensors are located symmetrically in an area of 90 mm by 90 mm, and have equal distances in both directions with respect to each other and to the boundary of the observed surface area. In Case 5 (Figure 4, right), the same four sensors are not distributed with relatively equal distances. Instead, the lengths of the intervals are ranked with ratio 1:2:1. The corresponding POD graphs obtained from MCS are shown in the left image of Figure 6. The results show that uniform (symmetric and equidistant) distribution of sensors has the highest $POD_{max}$.

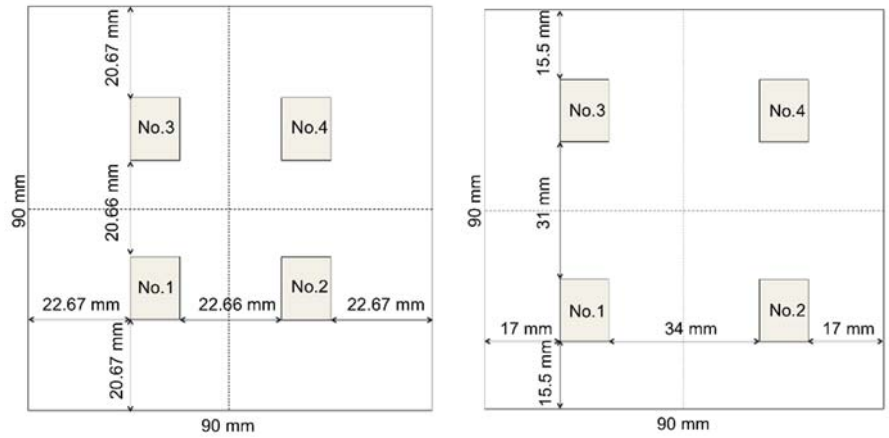


Figure 4. Left: Case 4, four sensors symmetrically and equidistantly distributed in the observed surface; Right: Case 5, four sensors symmetrically yet non-equidistantly distributed in the observed surface.

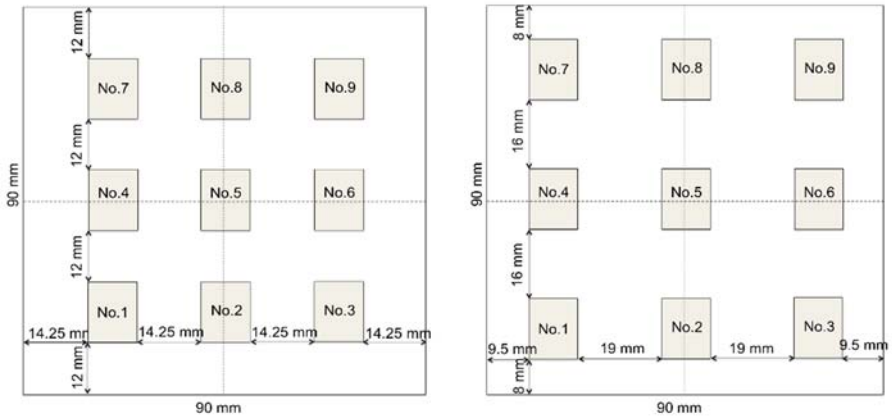


Figure 5. Left: Case 6, nine sensors symmetrically and equidistantly distributed in the observed surface; Right: Case 7, nine sensors symmetrically yet non-equidistantly distributed in the observed surface.

To further verify our conclusions obtained, the nine-sensor scenarios were studied. The total surface area is kept 90 mm by 90 mm. The uniform distribution of sensors was used in Case 6 and the distribution with the ratio 1:2:2:1 between distances in both directions is used in Case 7. The corresponding POD graphs obtained from MCS are shown in the right image of Figure 6. The results confirm that uniform (symmetric and equidistant) distribution of sensors has the highest $POD_{max}$.

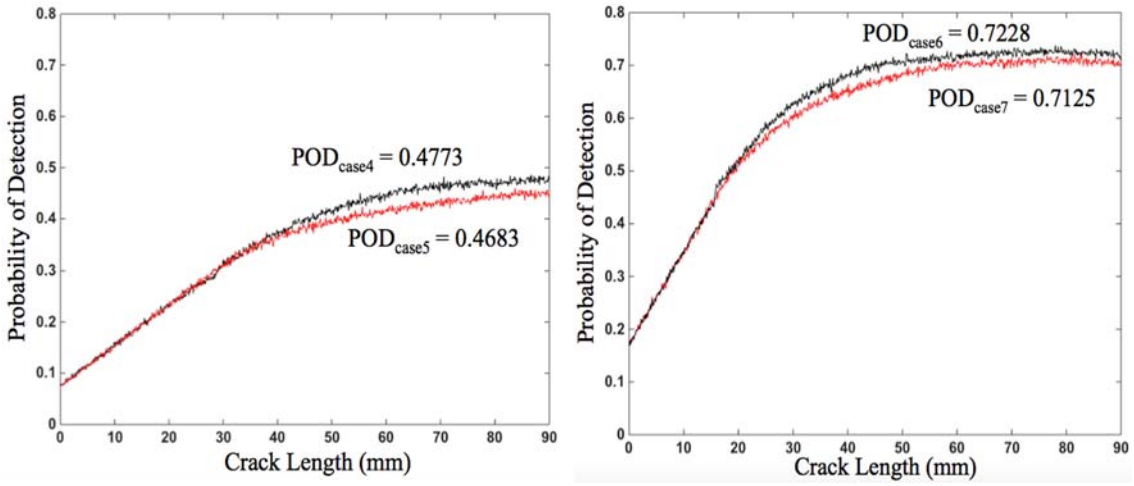


Figure 6. Left: PODs for four-sensor scenarios with different arrangements of sensors, Case 4 and Case 5; Right: PODs for nine-sensor scenarios with different arrangements of sensors, Case 6 and Case 7.

In summary, the outcome of this section is that the uniform, i.e., symmetric and equidistant distribution of sensors has the most effective POD.

Probability of Detection as a function of total sensor area

This section practically addresses the question “given the size of the sensing sheet and given the combined size of all the sensors, is it more efficient to use small amount of unit sensors with large areas, or large amount of unit sensors with small areas”. Since the latter would have a larger total perimeter of sensors, we anticipated that it would be more effective solution. We verified our hypothesis by MCS.

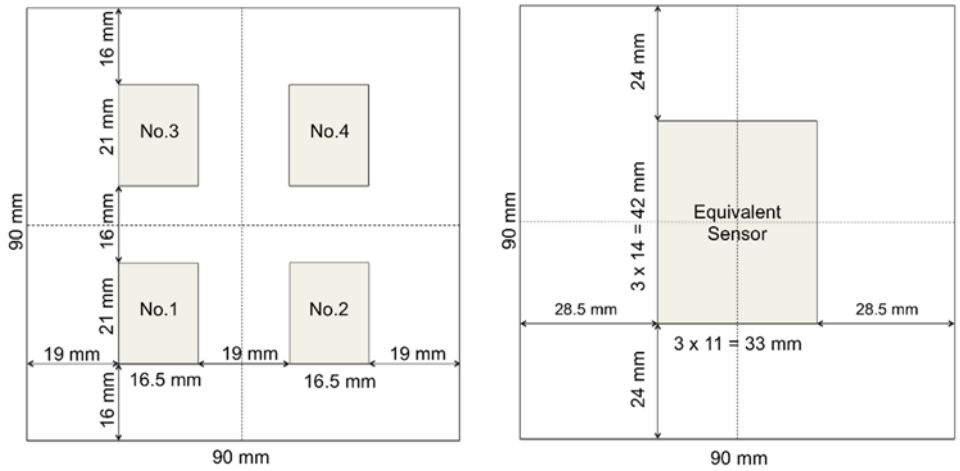


Figure 7. Left: Case 8, four (larger) sensors uniformly distributed in the observed surface; Right: Case 9, single (large) sensor placed in the center of the observed surface.

Case 8 consists of four uniformly distributed sensors and Case 9 consists of a single sensor placed in the center of the observed sensing sheet, as shown in Figure 7. The dimensions of the observed area are the same as for Cases 4-7 (90 mm x 90 mm). The total area of sensors is the same as for Case 6 (nine sensors of 11 mm x14 mm = 1386 mm$^2$), i.e., Case 8 has four sensors of 16.5 mm x 21 mm and Case 9 has single sensor of 33 mm x 42 mm. The ratio between sensor dimensions $b$ and $h$ is kept constant ($b$:$h$=11:14). The comparison of PODs for the three cases is given in Figure 8. The results show that the Case 6 (nine smaller sensors) is the most effective, while Case 9 (one large sensor) is the least effective.

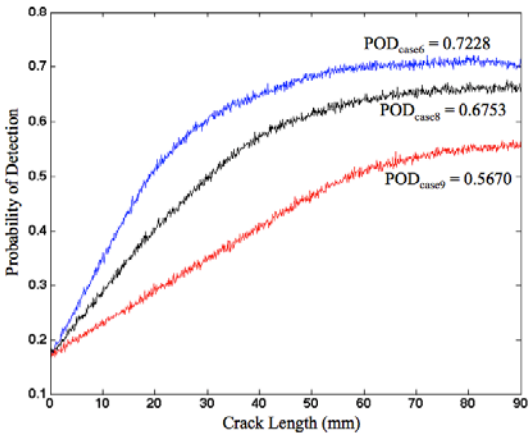


Figure 8. Comparison of PODs for Cases 6, 8 and 9.

This comparison thus confirmed our assumption that for a given total (combined) sensor area, the arrangement having more sensors with smaller individual areas has larger POD than arrangement consisting of less sensors with larger individual areas. Consequently, when designing the sensing sheet, it is important to follow this principle.

**Probability of detection for sensors with angular sensitivity**

Full-bridge resistive strain sensor has been selected as the unit sensor in sensing sheet due to its understood and proven functioning principle. It consists of four resistors oriented in two perpendicular directions and interconnected in a Wheatstone bridge configuration, as shown in Figure 9. It provides a differential strain signal, which improves robustness against temperature variations. Due to its bi-directional nature, there is a concern on its damage detection capabilities with regards to orientation of damage with respect to sensors. Consequently, the angular sensitivity is studied in this task.

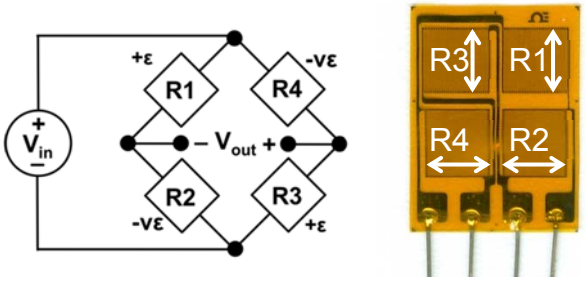


Figure 9. Schematic representation of Wheatstone bridge and full-bridge sensor with four resistors in Wheatstone bridge configuration (arrows show the direction in which the individual resistors are sensitive to strain).

*Evaluation of angular sensitivity of full-bridge strain sensor*

The main focus of this test was to examine the relationship between crack opening and measured strain for the full-bridge strain sensors, given an angel with respect to sensor. Since the cost of manufacturing prototypical sensing sheets is very high, less expensive commercial strain gauges were used in this study. This simplification is justified because similar sensors will be patterned on the aforementioned sensing sheets in the future. In order to achieve repeatable results, all experiments were conducted in a controlled laboratory environment with the same preparation and testing procedure. Each experiment involved mounting a small artificially cracked concrete slab to a micrometer stage and bonding a commercially available full-bridge sensor (total length = 14.8 mm) over the crack. High-strength epoxy was used in both the concrete-stage interface and the concrete-sensor interface. The micrometric screw attached to the stage controlled and adjusted the crack width, and strain readings were taken by appropriate reading unit. Experiments were stopped either when the strain sensor was broken or when the measuring range of the reading unit was overpassed. A schematic view to the test set-up is shown in Figure 10.


Figure 10. Left: top view of the experiment setup. Right: positioning of the sensor 90° to the crack (source: Tung et al. 2014, see journal papers in Conclusions).

In the frame of previous UTC research project (Tier I Final Report CAIT-UTC-025 Multi-Sensor Sheets Based on Large-Area Electronics for Advanced Structural Health Monitoring of Civil Infrastructure [6]), 90° angle was tested, i.e., the crack perpendicular to sensor's resistors R1 and R3 (see Figure 9) was created and its size varied. I total 10 tests were made, and the results are shown in Figure 11. The mean and standard deviations of results are shown in the figure in form of dashed lines.

Important conclusions from these tests ware that the crack results in extremely high strain reading on sensor, and while the best way to estimate the crack opening is to use probabilistic approach (lognormal distribution shown in Figure 11), an average sensitivity of sensor to crack opening is approximately equal to 31 με/μm.

In frame of this project, several tests were performed on cracked concrete specimens to infer how the damage orientation influences response of the sensor. An exhaustive set of six cases were studied with damage orientation as shown with dashed lines in Figure 12. Case A has been studied and described in the frame of previous UTC [6]. Cases B to F were studied in this research, and each test was repeated three times. The testing set-up was the same as in the previous project, and it is shown in Figure 12. Results of the tests are shown in Figure 13.

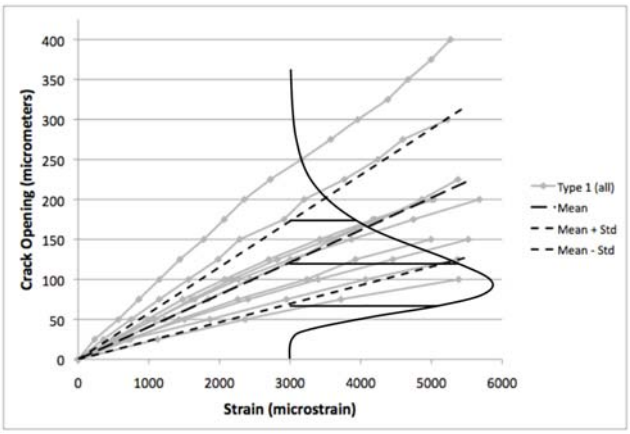


Figure 11. Crack opening vs. strain for Case A. Mean ± one standard deviation and lognormal distribution for the calibration coefficient shown (source: Tung et al. 2014, see journal papers in Conclusions).

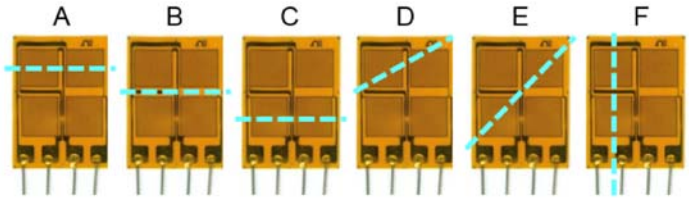


Figure 12. Tested positions of crack (dashed line) with respect to sensor (source: Glisic et al. 2016, see journal papers in Conclusions).

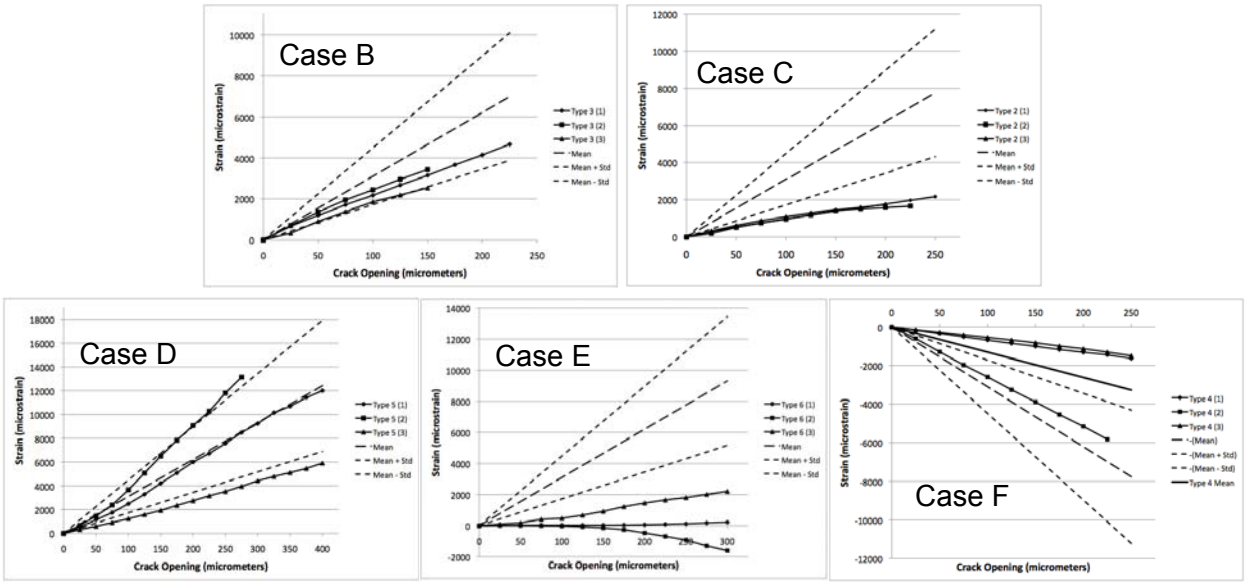


Figure 13. Crack opening vs. strain for Cases B-F. Mean ± one standard deviation of Case A shown for comparison purposes (source: Tung et al. 2014, see journal papers in Conclusions).

Mean and standard deviation from Case A are displayed on graphs in Figure 13, in order to compare each case with Case A, which is proven to be sensitive to crack opening. From the figures, it can be concluded that Cases A, B and D show similar sensitivity to crack, in average of 31 με/μm. This means that 0.01 mm crack will result in strain reading of approximately 310 με, which is clear indication of damage.

Cases C and F show approximately two times less sensitivity, and in addition, Case F has negative response, but their overall sensitivity to damage is still satisfactory: 0.01 mm crack will result in sensor reading of approximately 155 με, which is still clear indication of damage (typical live loads on the bridge rarely produce 100 με).

Case E is the only one that shows small sensitivity to damage. The three tests produced three different results, with one positive trend, one negative trend and one trend close to zero. Thus, this is the most unfavorable orientation of crack with respect to sensor. This issue can be addressed by patterning the sensors in a staggered arrangement, where there is a higher chance of crack detection for diagonal cracks, see Figure 14.

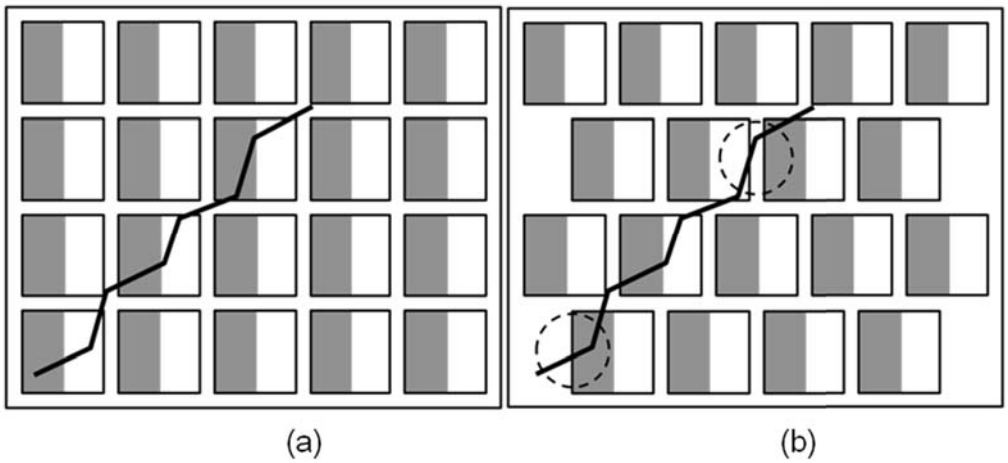


Figure 14. (a) A regular sensor arrangement has a higher probability of diagonal cracks being undetected, and (b) a staggered sensor arrangement is more likely to detect diagonal cracks.

However, the research in Task 1 (previous section) has shown that the highest POD is obtained for uniformly distributed sensors. Contribution of staggered configuration to the POD is evaluated in the next subsection.

*Determination of probability of detection using analytical and numerical methods*

For full-bridge sensor (see Figure 9), The relationship between the output/measured voltage signal (Vout) and the input/excitation voltage across the sensor (Vin) can be expressed in terms of the resistance of the four resistors:

$$V_{out} = \left( \frac{R_4}{R_3 + R_4} - \frac{R_1}{R_1 + R_2} \right) V_{in} \tag{2}$$

In this study, the initial resistance of each resistor is equal (R1 = R2 = R3 = R4 = R).

Therefore, substituting this into Equation 2 yields:

$$V_{out} = \left(\frac{1}{2} - \frac{1}{2}\right) V_{in} = 0 \tag{3}$$

When the sensor is exposed to strain or crack, one or more of the four resistors can be activated, which will in turn change the output voltage signal of the sensor. From Equations 2 and 3, we can derive an expression for change in output voltage $\Delta V_{out}$ in terms of changes in resistance of resistors ($\Delta R_1$, $\Delta R_2$, $\Delta R_3$, and $\Delta R_4$) caused by the strain or crack:

$$V_{out} + \Delta V_{out} = \Delta V_{out} = \left( \frac{R_4 + \Delta R_4}{R_3 + \Delta R_3 + R_4 + \Delta R_4} - \frac{R_1 + \Delta R_1}{R_1 + \Delta R_1 + R_2 + \Delta R_2} \right) V_{in} \tag{4}$$

In a non-strained sensor, $\Delta R_i = 0$, ($i$=1…4), and consequently $\Delta V_{out} = 0$ (see Equation 3). However, when the sensor is exposed to strain or crack, the values for activated $\Delta R_i \neq 0$. Let define gauge factor for one resistor as the ratio of relative change in electrical resistance to the relative change in length (strain):

$$GF = \frac{\Delta R / R}{\varepsilon} \tag{5}$$

Combining Equation 5 and Equation 4 yields:

(4)

$$\Delta V_{out} = \left( \frac{1 + GF\varepsilon_4}{2 + GF\varepsilon_3 + GF\varepsilon_4} - \frac{1 + GF\varepsilon_1}{2 + GF\varepsilon_1 + GF\varepsilon_2} \right) V_{in} \tag{6}$$

which can be rearranged as:

$$\Delta V_r = \frac{\Delta V_{out}}{V_{in}} = \frac{1 + GF\varepsilon_4}{2 + GF\varepsilon_3 + GF\varepsilon_4} - \frac{1 + GF\varepsilon_1}{2 + GF\varepsilon_1 + GF\varepsilon_2} \tag{7}$$

where $\Delta V_r$ is the voltage ratio (defined as the difference between strained and unstrained output voltage over the input voltage).

For sensor exposed to uniaxial stress, elements R1 and R3 measure the strain ($\varepsilon$) in the direction of stress, and elements R2 and R4 measure the strain perpendicular to direction of stress, due to Poisson's effect ($-\nu\varepsilon$). The relation between the voltage ration and strain in direction of stress is then calculated using the following expression:

$$\varepsilon = \frac{-2\Delta V_r}{GF[(\nu + 1) - \Delta V_r(\nu - 1)]} \tag{8}$$

Diagonal crack, i.e., Case E, affects resistors R1 and R4 equally. Therefore, substituting $\varepsilon_1 = \varepsilon_4 = \varepsilon_{crack}$ and $\varepsilon_2 = \varepsilon_3 = 0$ into Equation 7 yields:

$$\Delta V_r = \frac{(1 + GF\varepsilon_{crack})(1 - 1)}{2 + GF\varepsilon_{crack}} = 0 \tag{9}$$

which confirms the test results that sensor is not sensitive to crack with this orientation. The

same result is obtained when crack crosses resistors R2 and R3.

Important conclusion from the above derivation is that the sensor is not sensitive to crack only if the two terms on the right hand side of Equation 7 cancel each other. It can be proven, by deriving the expressions that the only two cases when this happens are the two mentioned above, diagonal crack over resistors R1 and R4 (Case E in Figure 12) and symmetric case, i.e., the crack over resistors R2 and R3.

While the two above cases are possible, their mathematical probability to happen is zero. Thus, these cases do not change the POD calculated in Task 1, and staggered configuration, from that point of view is not necessary.

**Probability of detection for strain distributions based on mechanical analytical models**

Results from the previous UTC grant [6] have shown that the response of the sensor to crack is different for concrete and steel. The main conclusion were:

- In the case of concrete structure, the sensor can survive, in average, a crack opening of 1.5 mm before it fails; this is due to degradation of crack mouth which enables redistribution of stress concertation in sensor over longer length;

- In the case of steel structure, the sensor fails as soon as it is intercepted by crack; this is due to the lack of degradation at the crack mouth.

Considerations regarding POD presented in the previous two sections of the report, assume that the sensor will survive the crack opening. All these considerations are valid in the event the sensor is broken by the crack, and actually, that case is closer to the theoretical assumptions made when defining the POD in the previous UTC grant [6].

However, having the sensor that can survive initial damage is particularly beneficial, since, besides the damage detection it can provide estimation of crack opening and its evolution over time. Once this is achieved for the case of steel structures, the analysis of the POD for strain distributions based on mechanical analytical models is practically the same for both concrete and steel structures. The only difference would come from the local fluctuations resulting from concrete inhomogeneity [10], but in overall (in average) the analysis is the same.

Thus, in this task, first the adhesive that will enable the sensor to survive on the steel structure is identified and tested. Then influence of strain distribution to the POD is studied.

*Identification of adhesive for applications on steel structures*

Three high-strength flexible adhesives were tested: 3M DP100, DP105 and DP125. Initially, they were tested on paper samples, to qualitatively assess viscosity, flexibility, and setting time. All three adhesives were very flexible and could be twisted and bent by hand, with virtually no effort. The 3M DP100 had a setting time of approximately 5 minutes, the DP105 of approximately 20 minutes, while the DP125 had a setting time which exceeded 30 minutes. Given that preferred setting time is neither too short (to give sufficient time to place the sensing sheet) nor too long (to avoid sheet's displacement caused by gravity or accidental contact shortly after placement), the DP125 adhesive was eliminated as having too long setting time,

and the two other adhesives were further tested.

First, the strain transfer enabled by the adhesives was tested. Three full-bridge strain gauges were glued to the top of a thin aluminum simply supported beam, which was subjected to three-point testing. The loading is performed using bottles filled with sand, denoted with B1, B2 and B3. The masses of bottles were 594.2 g, 598.1 g and 597.7 g, respectively. For each load step, the strain value was recorded using Omega DP41-5 gauge indicator. The total time of the test was less than two minutes, and measured room temperature was found to be stable. One sensor was glued using stiff Araldite adhesive, which was used in previous studies and thus it served as a reference. The two other sensors were glued using the 3M DP100 and 3M DP105. The aluminum beam with sensors used in the test is shown in Figure 15.

(a) (b)

Figure 15. Strain transfer test: (a) global view to bean with sensors, and (b) detail of sensors.

The results of the strain transfer test are compared with the analytical strain model in Figure 16. The first and last load steps in figure correspond to initial and final steps, without loading. The other steps correspond to gradual loading and unloading following the sequence B1, B1+B2, B1+B2+B3, B1+B2, B1. Figure shows that the Araldite adhesive consistently transferred the greatest fraction of strain from the structure to the sensor, while the two flexible adhesives transferred significantly less. However, there was no significant difference in strain transfer between the 3M DP100 and 3M DP105 adhesives, and both demonstrated ability to transfer the strain from the plate to the sensors.

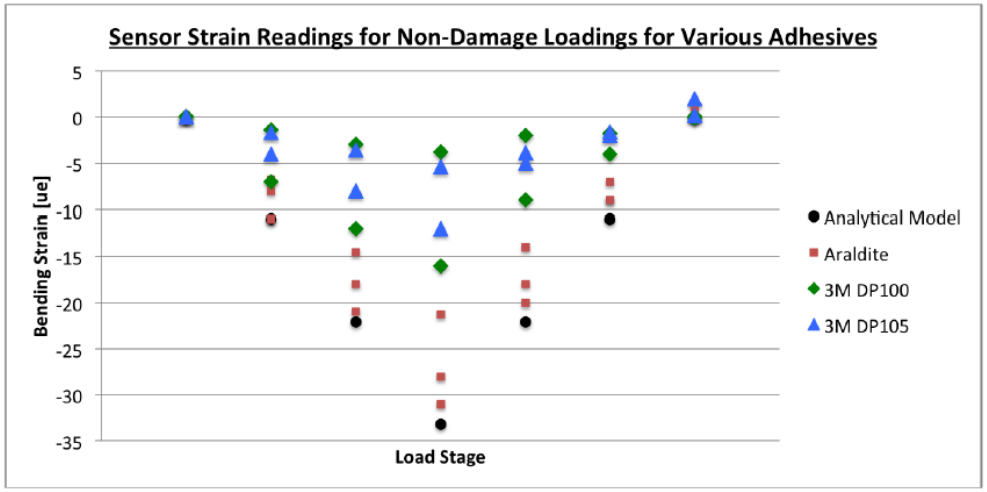


Figure 16. Results of strain transfer tests.

Once the quality of strain transfer was assessed, the sensor behavior under crack opening was evaluated. In each test a sensor was glued to “closed” aluminum plates and the adhesive was given time to cure. After adhesive reached suitable strength, an artificial crack was generated by pulling the aluminum plates apart in regular increments of 0.0001 inches. The strain readings were performed two times: the first time immediately after the crack opening increment was applied, and the second time five minutes later, to record the ”relaxed” sensor reading. Each test was stopped when the sensor could no longer read the strain or when the sensor debonded (whichever happened first). An example of the crack test presented above (following testing) is shown in Figure 17.

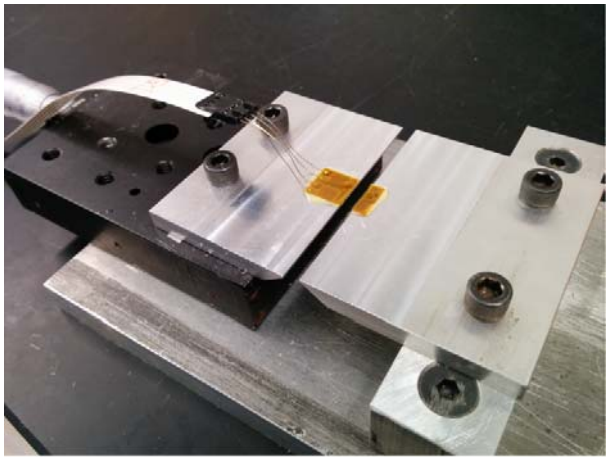

Figure 17. Crack opening test set-up (after the failure of the sensor).

Figures 18 and 19 show the results for the 3M DP100 adhesive. In the first test (Figure 18) the adhesive was allowed to cure for 24 hours, while in the second test it was allowed to cure for 72 hours (Figure 19). These time-dependent tests were performed in order to assess the adhesives’ performance with time and establish a minimum cure time.

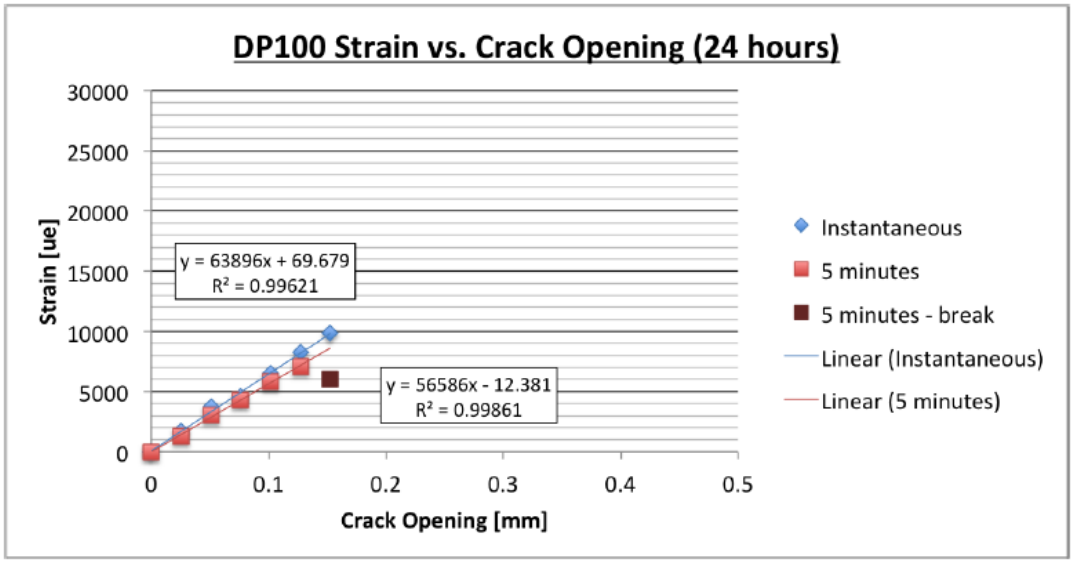


Figure 18. Test with DP100 adhesive cured for 24 hours, crack opening vs. strain.

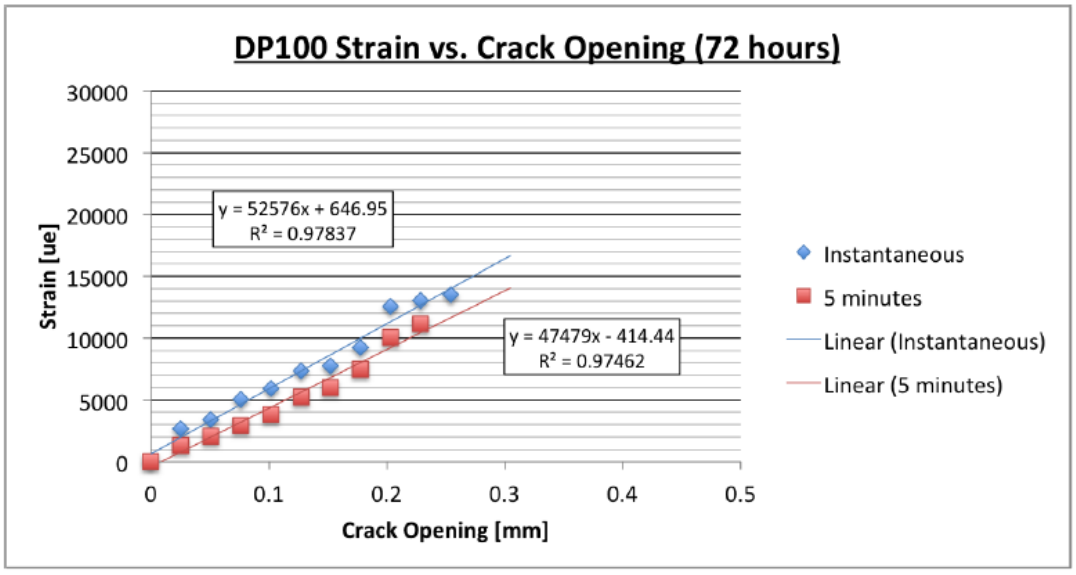


Figure 19. Test with DP100 adhesive cured for 72 hours, crack opening vs. strain.

The test showed that the slopes in two tests were different which is probably due to difference in thickness of the adhesive applied. However, important difference is in bond strength: the sensor glued with 24-hour cured DP100 showed readings up to a crack opening of approximately 0.15 mm, whereas the test with 72-hour cured DP100 showed readings up to approximately 0.26 mm crack. Hence, the adhesive performs better when cured for longer time.

Similar tests were performed with the DP105 adhesive, and the results are shown in Figures 20 and 21.

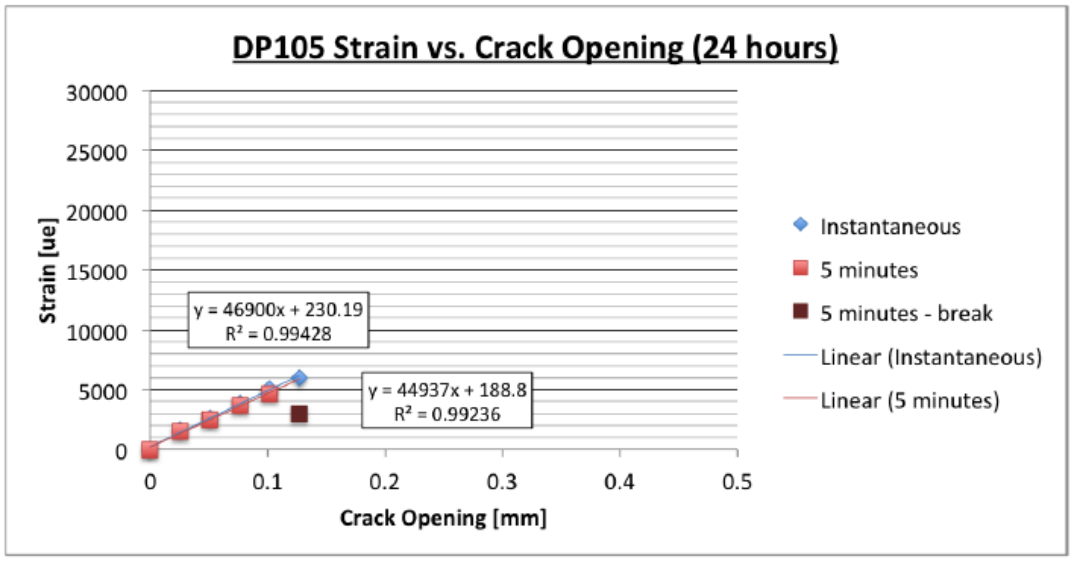


Figure 20. Test with DP105 adhesive cured for 24 hours, crack opening vs. strain.

.

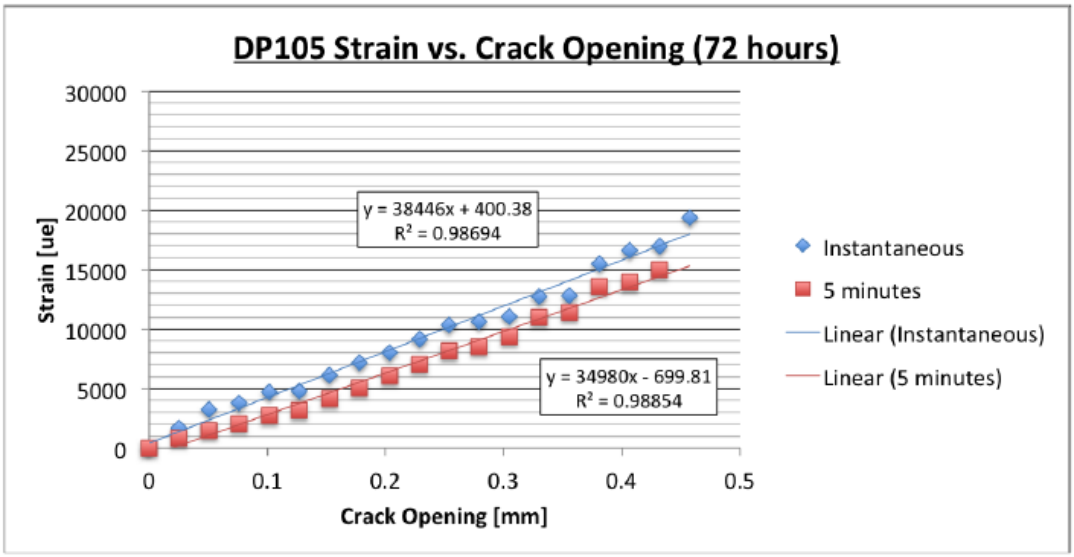


Figure 21. Test with DP105 adhesive cured for 72 hours, crack opening vs. strain.

Similar to the results of test with DP100 adhesive, the results of test with DP105 adhesive showed similar inconsistency of slopes with time. However, the test confirmed that longer cure provide better bonding, and in addition, sensor glued with DP105 adhesive continued to read strain for crack openings up to 0.45 mm, which is almost double compared to the sensor glued with DP100 adhesive. Therefore, the DP105 adhesive is considered the more suitable for applying sensing sheet onto the steel structures.

*Analysis of POD based on analytical strain model*

A sensing sheet measures the strain field at the surface to which it is installed. In most applications in bridge engineering, the state of stress is plane, and the strain in the sensor measures the strain in the plane of stress. The stresses in beams are caused by normal force $N$, shear force $S$ and bending moments $M_z$ and $M_y$, and the following formulas are used to calculate them:

$$\sigma_x(x,y) = \frac{N(x)}{A(x)} - \frac{M_z(x)}{I_z(x)}y + \frac{M_y(x)}{I_y(x)}z \tag{10a}$$

$$\sigma_y = 0 \tag{10b}$$

$$\tau_{xy}(x,y) = \frac{S_y(x)m(y)}{w(x,y)I(x)} \tag{10c}$$

where $x$-axis is along the centroid, $y$-axis is perpendicular to $x$-axis in the plane of stress, and $z$-axis is perpendicular to the plane of stresses; $z$ is distance of the observed plane from the centroid in the direction of $z$-axis; $m(y)$ is static moment of the surface below $y$, and $w$ is the width of the cross-section at point $(x,y)$.

For the plane state of stress in beams, at every point in the structure two principal axes and principal stresses $\sigma_1$ and $\sigma_2$ with respect to these axes can be found using the following

expressions:

$$\sigma_{1,2} = \frac{\sigma_x + \sigma_y}{2} \pm \sqrt{\left(\frac{\sigma_x + \sigma_y}{2}\right)^2 + \tau_{xy}^2} = \frac{\sigma_x}{2} \pm \sqrt{\left(\frac{\sigma_x}{2}\right)^2 + \tau_{xy}^2} \tag{11}$$

Important conclusion from Equation 11 is that for loaded beam structure $\sigma_1$ and $\sigma_2$ cannot be equal, as the expression under the square root is equal zero only if all stress components are equal zero. Moreover, if shear is present, than principal stresses must have opposite sign (one is in tension the other in compression). If shear is null, then one principal stress is null too.

Principal strains will have the same principal axes and the relationship between principal strain components $\varepsilon_1$ and $\varepsilon_2$, and principal stress components $\sigma_1$ and $\sigma_2$ is given in Equation 12.

$$\varepsilon_{1,2} = \frac{\sigma_{1,2}}{E} - \nu \frac{\sigma_{2,1}}{E} \tag{12}$$

where $E$ is Young modulus of elasticity and $\nu$ is Poisson's coefficient.

Let assume that the full-bridge sensor is oriented so that the sensing axes of resistors R1 and R3 are parallel to the first principal axis of strain and resistors, and the sensing axes of resistors R2 and R4 are parallel to the second principal axis of strain. In that case, Equation 7 transforms into:

$$\Delta V_r = \frac{\Delta V_{out}}{V_{in}} = \frac{1 + GF\varepsilon_2}{2 + GF\varepsilon_1 + GF\varepsilon_2} - \frac{1 + GF\varepsilon_1}{2 + GF\varepsilon_1 + GF\varepsilon_2} = \frac{GF(\varepsilon_2 - \varepsilon_1)}{2 + GF(\varepsilon_1 + \varepsilon_2)} = \frac{GF(\sigma_2 - \sigma_1)(1+\nu)}{2 + GF(\sigma_1 + \sigma_2)(1-\nu)} \tag{13}$$

Equation 13 shows that the sensor installed along the principal stress and strain axes will not be sensitive to strain only if $\varepsilon_1 = \varepsilon_2$, i.e., $\sigma_1$ and $\sigma_2$ (Equation 12), which based on Equation 11 cannot happen. In the other words, sensor installed along the principal axes will always be sensitive to strain, and consequently, in the case of cracking, it will be sensitive to cracking.

Now, let assume that the sensor is tilted for angel $\varphi$ with respect to principal axes. Then the stresses and strains in directions $n$ and $l$ with angle $\varphi$ with respect to the first and second principal axes are the following:

$$\sigma_n = \sigma_1 \cos^2\varphi + \sigma_2 \sin^2\varphi \tag{14a}$$

$$\sigma_l = \sigma_1 \sin^2\varphi + \sigma_2 \cos^2\varphi \tag{14b}$$

$$\varepsilon_n = \sigma_1(\cos^2\varphi - \nu\sin^2\varphi) + \sigma_2(\sin^2 - \nu\cos^2\varphi) \tag{14c}$$

$$\varepsilon_l = \sigma_1(\sin^2\varphi - \nu\cos^2\varphi) + \sigma_2(\cos^2 - \nu\sin^2\varphi) \tag{14d}$$

Finally, substitution of Equations 14c and 14d in Equation 7 yields:

$$\Delta V_r = \frac{\Delta V_{out}}{V_{in}} = \frac{1 + GF\varepsilon_l}{2 + GF\varepsilon_n + GF\varepsilon_l} - \frac{1 + GF\varepsilon_n}{2 + GF\varepsilon_n + GF\varepsilon_l} = \frac{GF(\varepsilon_l - \varepsilon_n)}{2 + GF(\varepsilon_n + \varepsilon_l)} = \frac{GF(\sigma_2 - \sigma_1)(1+\nu)\cos 2\varphi}{2 + GF(\sigma_1 + \sigma_2)(1-\nu)} \tag{15}$$

Equation 15 is practically $\cos 2\varphi$-mulitple of Equation 13. It shows that sensitivity to strain of a sensor with an angle $\varphi$ with respect to principal axes decreases proportionally with factor $\cos 2\varphi$, and when angle $\varphi$ is equal 45° the sensitivity is null. Other conclusion is that the maximum sensitivity is obtained when the angle $\varphi$ is equal 0°. Thus, when the angle $\varphi$ is close or equal to zero, the sensitivity to strain can significantly decrease, or vanish. However, sensitivity to crack will only vanish if the latter occurs exactly as shown for Case E in Figure 12. In the previous section we have demonstrated that the probability of this event is zero, and thus the POD functions remain unaffected.

**Validation**

Validation of POD approach developed in the first two tasks was validated by comparison with numerical simulations. Task 3 was validated by comparison with data-sets from the large-scale laboratory test performed in frame of the previous UTC [6].

*Comparison with numerical simulations*

The conclusion of Task 2 was that the orientation of the sensor with respect to crack does not significantly influence the POD. That is the reason why the first two subtasks are merged here.

Crack propagation is observed on an FEM simulation. In the simulation, a simply supported beam with notch is loaded in the middle of the span. Stress concentration at the notch creates the crack that propagates with the increase of the load. Stress concertation and crack propagation are shown in the sequence of images shown in Figure 22.

Figure 22 shows that the crack mostly follow the line of biggest principal stress. For the specific case shown in Figure 22, the crack line first departs from the notch in a random direction, and then quickly it takes a shape of quasi-straight line that is perpendicular to the line of maximal tensional stress.

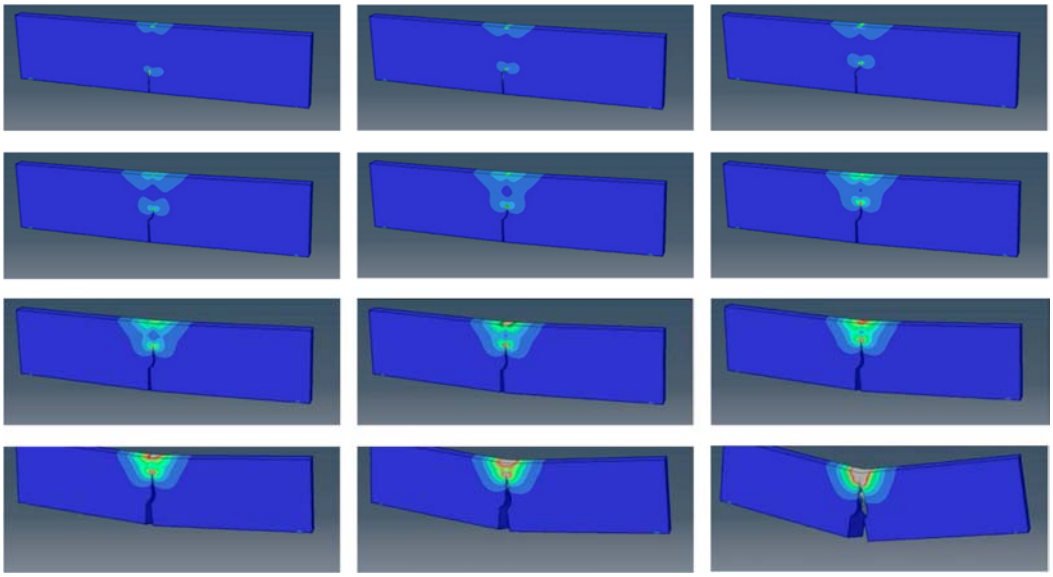

Figure 22. Numerically simulated sequence of stress concentration and crack propagation.

Assuming that the crack is detected only when it directly affects the sensor, various designs of sensing sheet were layered over the simulated crack and their capabilities to detect the crack were evaluated. Since the problem was again reduced to the problem of geometrical probability, the results similar to those presented in Tasks 1 and 2 are obtained.

However, an important difference is noticed: numerical simulation has shown that even the sensors that are not in direct contact with the crack can actually detect the damage. This is due to stress decay after the crack "passed" nearby the sensor. This is observation is schematically shown in Figure 23.

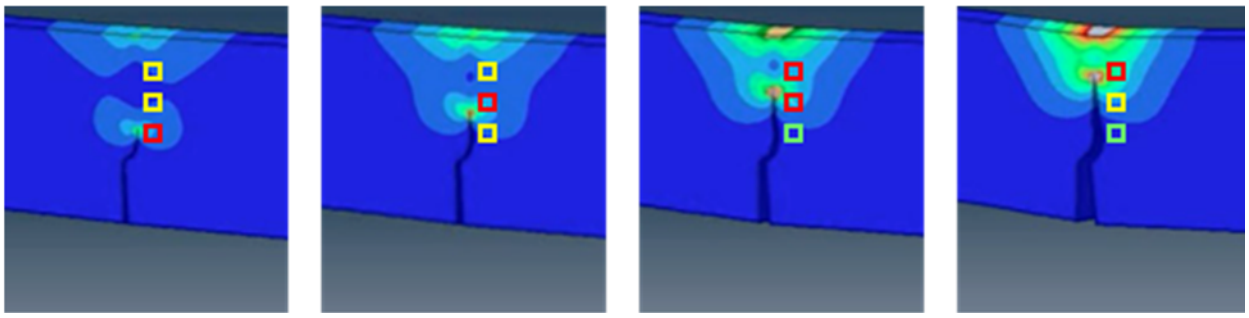

Figure 23. Change in strain in three sensors, shown as squares, installed nearby the crack;

In Figure 23, red color of the square symbolizing the sensor indicates that the sensor is under high strain, yellow indicates that the sensor is under moderate strain, and yellow that the sensor is under very low or no strain.

Thus, as the final conclusion, since even the sensors that are not in direct contact with crack can also detect the damage, the POD calculated in Tasks 1 and 2 should be considered rather as a conservative lower limits of the POD.

*Comparison with data from laboratory tests*

Laboratory tests were performed in frame of UTC Tier I project, see [6]. To avoid repetition, the tests are not described in detail in this report. However, to better follow this section, a relevant brief description is given. Tests consisted of installing prototype of sensing sheet onto notched steel specimen exposed to cycling loading. Cycling creates fatigue, which in turn results in crack that was detected by sensing sheet.

In order to decrease the cost of manufacturing of the sensing sheet prototypes, it was decided to proceed with the hybrid solution, i.e., to pattern the interconnect of the sensing sheet and then to laminate commercially available strain sensors onto the interconnect. The interconnect allowed multiple sensors arranged on the sensing sheet to be connected with the reading unit. The size of the sensing sheet prototypes is determined based on the dimensions of large-scale steel test specimens, shown in Figure 24 (see also Figure 26). The steel specimen in Figure 24 represents a compact specimen according to ASTM E647-08. In total two arrangements of individual sensors denoted as SS1 and SS2 were considered, as shown in Figures 25. The strain sensing sheets were 6 x 6 inch, and accommodated for 31 individual strain sensors in both cases.

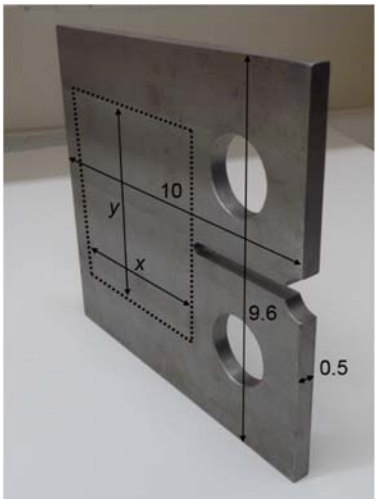


Figure 24. Photo of the steel test specimen according to ASTM E647-08. The area within the dotted line represents the location of the prototype multi-sensing sheet. Dimensions in inches [6].

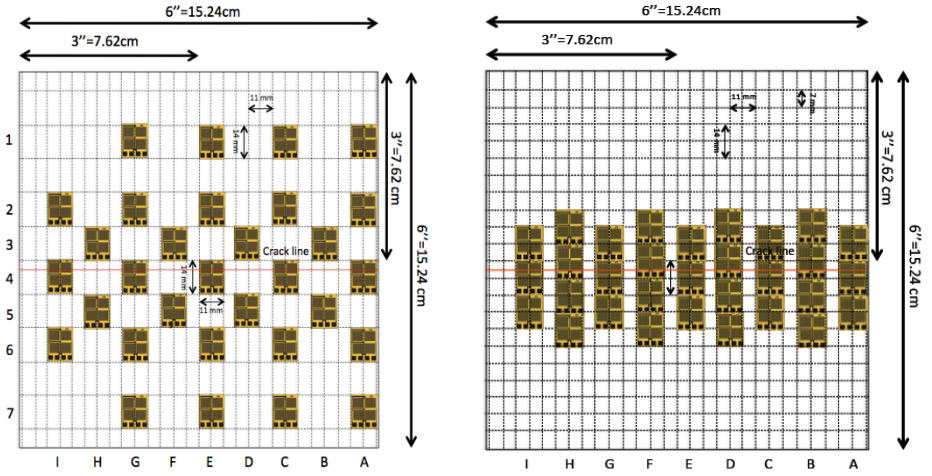


Figure 25. Left: Disperse arrangement of sensors (design "SS1"). Right: Dense arrangement of sensors (design "*SS2*"). In tests, the crack propagates from "*A*" towards "*I*" [6].

During the cycling tests the tip of the notch zone in the steel plate would suffer the largest stress concentration, and the initial fatigue crack was expected to occur at that location. Based on the four test observations, the initial crack appeared before 40,000 cycles are carried out. Given that the crack orientation and location was known, and certainty that the first sensor in contact with notch will immediately detect the crack, the POD=1 regardless the length of the crack. Thus, to evaluate the approach, it was decided to rather evaluate POD of crack propagation, i.e., to see if possible to infer the length of the crack as it progresses. Based on designs, it was clear that for design SS1, the length of the crack should be two times longer than for design SS2, to be detected by the next individual sensor. Thus, SS1 was two times less likely to detect propagation of the crack.

Figure 26 shows the initial cracks in Specimens No. 1 and 2. Under the cycling that followed

the initiation, the crack propagation was very slow and it started to propagate faster only when the specimen was close to failure. The specimen was considered as failed when the vertical distance between the two fixture pins had reached one inch, and at that stage the crack ended in the area close to the middle of the plate.

Figure 27 shows the examples of the failure of the sensing sheets under extreme crack opening. Two main mechanisms of the sheet failure were noticed: delamination and tearing. It is important to note that as the initial crack crossed the first closest sensor, this sensor would be damaged immediately. However, the other sensors would continue functioning until either they are damaged or the interconnect is damaged by one of the above presented failure modes.

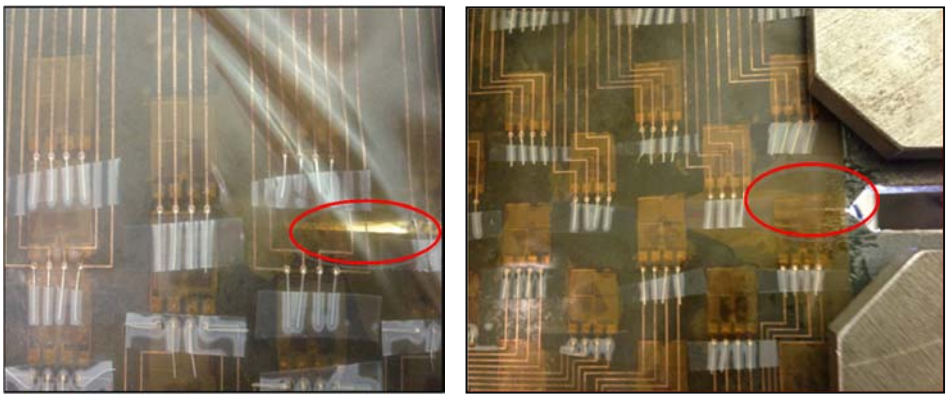

Figure 26. Initial crack occurring in Specimen No. 1 (left) and No. 2 (right) [6].

.

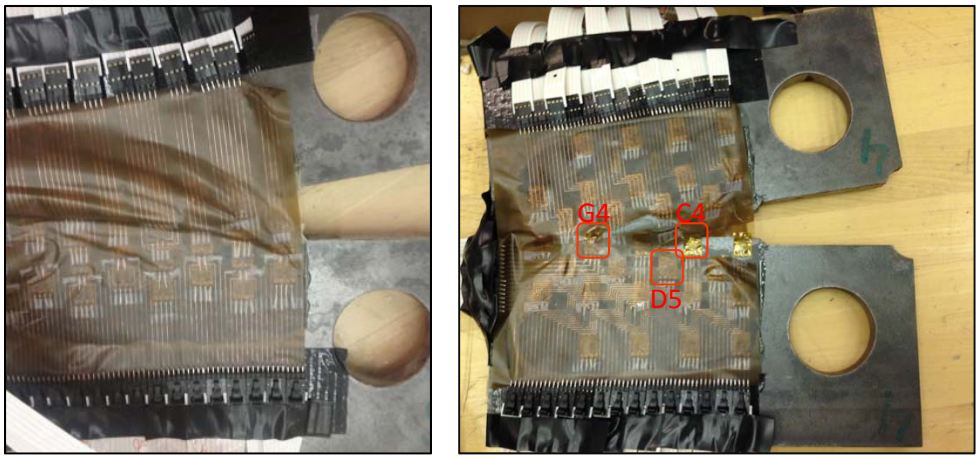


Figure 27. Typical failure modes of the sensing sheet under excessive crack opening; Left: delamination, Sample No.; 3; Right: tearing, Specimen No. 4 [6].

To illustrate the general response of strain sensors from the sensing sheets, three typical individual sensors from Specimen No. 4 are presented in Figure 28. The selected examples are sensors with coordinates *C4*, *D5* and *G4* and these sensors are encircled in Figure 26.Note that crack propagates from side *A* towards *I* (see Figure 6) i.e., it first meets sensor with coordinate *C* and then propagates towards the sensors with coordinates *D* and/or *G*. Figure 26 shows that the sensor *C4*, which was on the crack, was clearly broken by it; sensor *D5* is not at the location of the crack, but below it, and thus it was not damaged by crack; finally, sensor *G4* was on the crack propagation line, and the crack tip reached it, so this sensor was damaged.

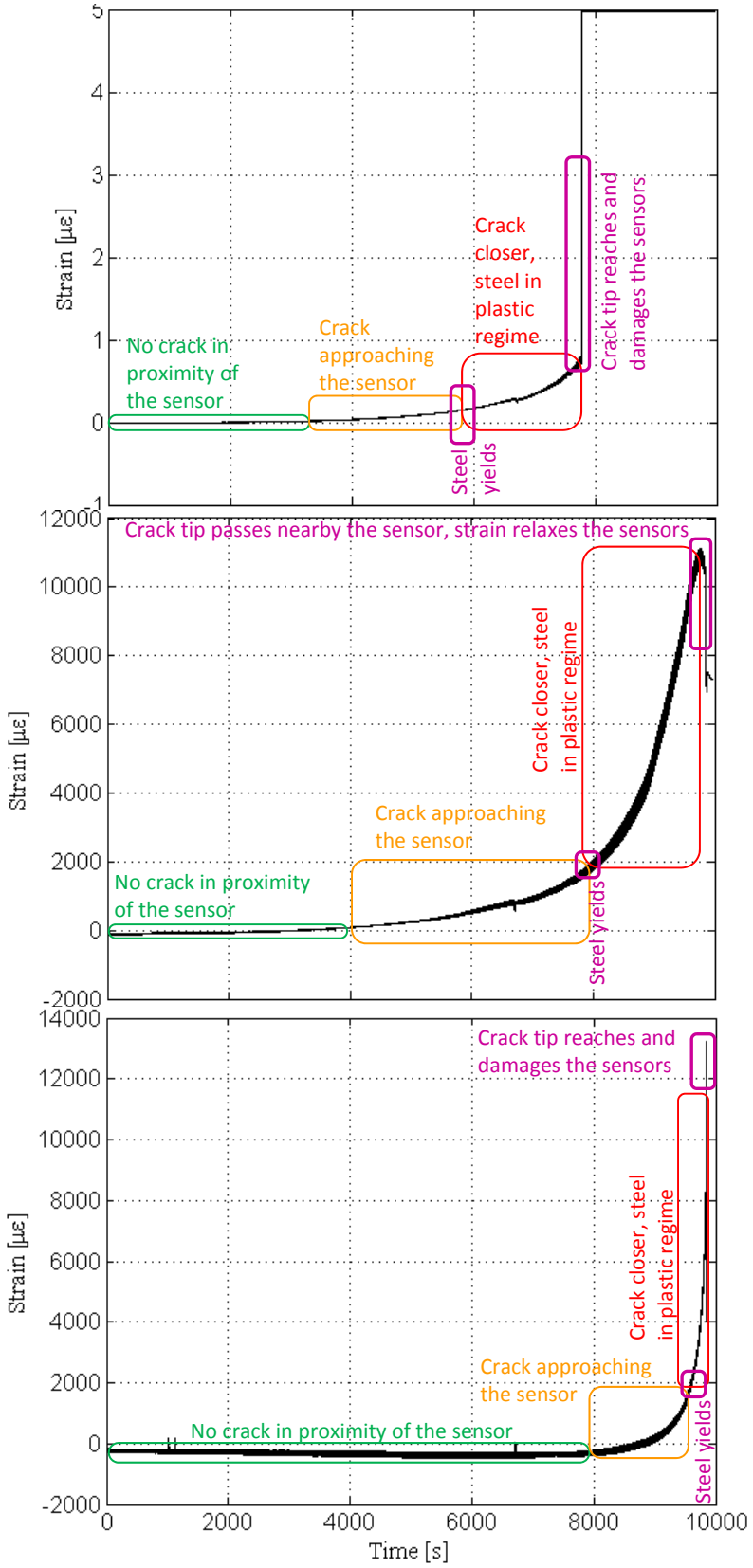


Figure 28. Typical sensor readings, Specimen No. 4 [6].

Figure 28 shows that the sensors that were in contact with the crack would be immediately damaged, and this failure of sensors was used as indication of crack propagation. In case of design SS2, this mechanism enabled detection of crack propagation as predicted.

Nevertheless, while design 2 had benefits of denser sensor array, the design 1 was also successful in damage detection and evaluation, indirectly, through relaxation of sensors, as shown in middle graph of Figure 28. This is a very important as it shows that even less dense networks could be successful in damage characterization, which may significantly simplify manufacturing of sensing sheets and data analysis. Actually, the performance of sheets SS1 and SS2 was the same, despite the theoretical POD being less favorable for design SS1. This shows that theoretical POD is rather conservative estimation, and its more accurate determination should be a subject of future research.

The tests have demonstrated that the sensing sheet could perform reliable crack detection and could follow crack propagation in-time. This is important finding as it proves the concept of direct sensing applied to dense arrays of strain sensors, and validates the idea of the sensing sheet. In addition, the tests helped identify several directions for future research.

## CONCLUSIONS

Several major conclusions can be drawn from this project:

1. The literature review revealed that Probability of Detection (POD) is viable approach for evaluating damage detection systems, but no application of POD was found for two-dimensional (surface) sensors. These findings further justified this project.

2. POD for single sensor scenario can be derived analytically. However, for multi-sensor cases a Monte Carlo simulation had to be developed. Exhaustive study regarding arrangement of sensors was performed, taking into account arrangement of sensors, arrangement of empty spaces between the sensors, and relative size of area of the sensing sheet covered by sensors. The following conclusions were carried out from the above study:
    a. With assumption that the sensor can detect the crack only when in direct contact with it, the max. POD is obtained when the sensors and empty spaces are uniformly distributed over the sheet.
    b. With the same assumption, for given relative size of the area covered by sensors with respect to sensing sheet, the POD is higher if larger amount of small-sized sensor is used, as opposed to the use of smaller amount of large-sized sensor, in which case the POD is smaller.

3. Resistive strain sensor in the full-bridge configuration was chosen for strain sensor as its differential sensing characteristics minimize the noise from environment. This sensor has two main resistors (R1 and R3) oriented in one direction, and two other accessory resistors (R2 and R4) oriented in perpendicular direction. Exhaustive set of tests was designed and performed in order to evaluate the detection capabilities of the sensor in the case the damage has an angle with respect to two main resistors of the sensor. The

following was concluded:

a. For three positions of the crack with respect to sensor, the sensitivity to crack is highest: crack perpendicular to main resistors (Case A); crack between the main and accessory resistors (Case B); and crack angled with respect to main resistors, but not affecting the accessory resistors (Case D),.
b. For two positions of the crack with respect to sensor, the sensitivity to crack is approximately two times lower than in the above case; however, the sensitivity is still very high and the sensor can be used for crack detection these cases: crack perpendicular to the main resistors, but affecting only the two accessory resistors (Case C); and crack parallel to main resistors, but affecting only one main and one accessory resistor (Case F). Case F shows negative response, which is not an issue for crack detection.
c. The only crack position that is unfavorable is when the crack occurs exactly diagonally over the one main and one accessory resistor (Case E). However, the probability of the crack occurring exactly at that location is null, thus this case can be disregarded in practical applications.

4. Results from the previous UTC grant [6] have shown that the in the case of concrete structure, the sensor can survive, in average, a crack opening of 1.5 mm before it fails, due to degradation of crack mouth which enables redistribution of stress concertation in sensor over longer length. In the case of steel structure, the sensor fails as soon as it is intercepted by crack, which is due to the lack of degradation at the crack mouth.

   In this research a soft adhesive was successfully identified and tested, such that it enables sensor to survive the crack opening and provides the sensor response similar to that of the sensor installed on concrete. The soft adhesive has relatively low performance in strain transfer from the steel to the sensor, but this unfavorable effect does not affect damage detection capabilities of the sensor.

5. Analytical expressions based on solid mechanics shows that sensitivity of a full-bridge sensor to strain is the largest when the main and accessory resistors are oriented in the directions of stress and strain principal axes. As the angle of main and accessory resistors changes towards 45°, the sensitivity decreases, and becomes null for angle of 45°. However, sensitivity to crack (as opposed to strain) will only vanish if the latter occurs exactly diagonally over one main and one accessory resistor. In the above Point 3c we concluded that the probability of this event is zero, and thus the POD remains unaffected.

6. Numerical simulations and laboratory tests demonstrated that even the sensors that are not in direct contact with crack can also detect the damage. Thus, the POD calculated in Tasks 1 and 2 should be considered rather as a conservative lower limits of the POD.

7. In overall the results of the project are satisfactory. The concept of POD was studied and understood for the two-dimensional sensing sheets, and provided for guidance on arrangement of the unit sensors within the sheet. Several publications resulted from the project (see below), and recommendations for future research are identified and presented in the next section.

Publications resulting from the project:

Journal Papers

1. Tung, S-T., Glisic, B., (2016). Sensing sheet: the response of full-bridge strain sensors to thermal variations for detecting and characterizing cracks, Measurment Science and Technology, 27, art no. 124010 (16pp).

2. Glisic, B., Yao, Y.,Tung, S-T., Wagner, S., Sturm, J.C., Verma, N. (2016). Strain Sensing Sheets for Structural Health Monitoring based on Large-area Electronics and Integrated Circuits, Proceedings of the IEEE, 104(8): 1513-1528.

3. Yao, Y., Glisic, B. (2015). Sensing sheets: Optimal arrangement of dense array of sensors for an improved probability of damage detection, Structural Health Monitoring, 4(5):513-531.

4. Yao, Y., Glisic, B. (2015). Detection of steel fatigue cracks with strain sensing sheets based on large area electronics, Sensors, 15: 8088-8108.

5. Tung, S-T., Yao, Y., Glisic, B. (2014). Sensing Sheet: The Sensitivity of Thin-Film Full-Bridge Strain Sensors for Crack Detection and Characterization, Measurement Science and Technology, 25(7), art. no. 075602 (14pp).

6. Yao, Y., Tung, S-T. E., Glisic, B. (2014). Crack detection and characterization techniques – an overview, Structural Control and Health Monitoring, 21(12): 1387–1413.

Conference papers:

1. Yao, Y., Glisic, B. (2016). Detection of Steel Fatigue Cracks with Strain Sensing Sheets Based on Large Area Electronics, 8th European Workshop On Structural Health Monitoring (EWSHM 2016), Spain, Bilbao.

2. Yao, Y., Tung, S-T.E., Verma, N., Wagner S., Sturm, J., Glisic, B. (2015). Large-area electronics combined with integrated circuits into a strain sensing sheet, Proceedings of IABSE Conference 2015, Geneva, Swizerland, September 23-25, 2015.

3. Glisic, B. (2015). Very Dense Arrays of Sensors for Reliable and Accurate Damage Identification, 7th International Conference on Structural Health Monitoring of Intelligent Infrastructure (SHMII-7), Turin, Italy, July 1-3, 2015 (invited keynote paper).

4. Yao, Y., Glisic, B. (2015). Detection of steel fatigue cracks with strain sensing sheets based on large area electronics, 7th International Conference on Structural Health Monitoring of Intelligent Infrastructure (SHMII-7), Turin, Italy, July 1-3, 2015.

5. Yao Y., Glisic, B. (2015). Sensing sheets based on large area electronics for fatigue crack detection, Proc. of SPIE - The Int'l Society for Optical Engineering 9435-15.

6. Yao, Y., Glisic, B. (2014). Probabilistic Damage Detection Based on Large Area Electronics Sensing Sheets, 7th European Workshop on Structural Health Monitoring (EWSHM), Nantes, France, July 8-11, 2014, paper on conference CD.

7. Yao, Y., Tung, S-T., Glisic, B. (2014) High-resolution sensing sheet for damage detection based on large area electronics, The 7th International Conference on Bridge Maintenance, Safety and Management (IABMAS), Shanghai, China, July 7-11, 2014, paper on conference CD.

8. Tung, S-T.E., Yao, Y., Glisic, B. (2014). Crack identification based on thin-film full-bridge strain sensors, Proceedings of SPIE - The International Society for Optical Engineering 9061 - 33.

## RECOMMENDATIONS

This project created methodology for evaluating probability of detection (POD) of a crack of a given size by sensing sheet with given configuration of sensors, assuming that crack occurrence over the area of sheet has uniform distribution. Performance and application of POD was explored and provided for guidance on arrangement of the unit sensors within the sheet. Also guidance for future research is inferred. The following recommendations are proposed based on experience and test results from the project:

1. Arrangement of unit strain sensor: to obtain maximum POD with given number of unit sensors, they should be uniformly (equidistantly) distributed in both directions (x and y), as shown in Figures 4-Left, and 5-Left.

2. Size of unit strain sensor: to obtain maximum POD with given total combined size of sensor areas, it is more effective to use larger number of smaller sensors, than smaller number of larger sensors.

3. Determination of POD and design of sensing sheet: POD of a sensing sheet with given characteristics can be determined using scaled curves shown in Figures 3, 6 and 8; inverse procedure can be used to design sensing sheet with desired POD; however, the above theoretical values of POD are rather conservative, as the sensors need not to be in direct contact with unit sensors to detect the damage; more accurate determination of POD would require future research.

4. Angle of unit sensor with respect to crack: while angle of unit sensor with respect to crack influences sensitivity in evaluation of crack size, it does not influence significantly the performance of crack detection; while the best results in crack opening evaluation can be obtained by orienting the individual sensors in direction of principal stresses, simple crack detection capability is not in general influenced by orientation of sensors.

5. Selection of adhesive: due to the fact that the steel does not degrade at crack mouth, and given that the accuracy in strain monitoring is not of interest for sensing sheet (it uses the strain to detect the crack, but accurate strain measurement is not necessary), a soft adhesive should be used when applying sensing sheet to the steel structures; this will enable the unit sensors to survive initial crack opening, and help evaluate its size; in case of concrete, stiff adhesive can be used; future research might show if there is any

benefit in using soft adhesive for application of sensing sheet to concrete structures.

6. Future research: the main direction for future research would be towards more accurate evaluation of POD, taking into account that sensors that are not in direct contact, but only in close proximity of crack, can detect the damage; it would be of particular interest to establish how large is “sensor influence zone”, i.e., what is maximum distance between sensor and crack, so that the sensor can reliably detect the crack; another (smaller) area of research would be evaluation of soft adhesives applied to concrete structures.

## REFERENCES


1. ASCE. Report Card for America's Infrastructure. 2010 [cited 2010 11/04]; Available from: http://www.infrastructurereportcard.org/.

2. USDOT, Transit State of Good Repair - Beginning the Dialogue. 2008, Federal Transit Administration.

3. Window, A.L., Strain Gauge Technology. 1992, London, UK: Springer.

4. IWSHM. Proceedings. in The 9th International Workshop on Structural Health Monitoring (IWSHM). 2013. Palo Alto, CA.

5. SHMII. Proceedings. in 6th International Conference on Structural Health Monitoring of Intelligent Infrastructure (SHMII-6). 2013. Hong Kong, China.

6. Glisic, B., Schumacher, T., Betti, R. (2014). COLLABORATIVE PROPOSAL: Multi-Sensor Sheets Based on Large-Area Electronics for Advanced Structural Health Monitoring of Civil Infrastructure, Project Report, CAIT- UTC-025.

7. Achenbach, J. D. and Kulkarni, S. S. (2008). “On the probability of an undetected surface-breaking crack.” Theoretical Applied Mechanics, Vol. 35, No. 1-3 pp. 1-10.

8. Cohen, M. L., Kulkarni, S. S., and Achenbach, J. D. (2012). “Probabilistic approach to growth and detection of a truncated distribution of initial crack lengths based on Paris’ Law.” Structural Health Monitoring, Vol.11, No.2, pp. 225-236.

9. Fujimoto, Y., Swilem, A. M., and Iwata, M. (1990). “Estimation of Probabilities of Crack Detection and False Indication in Visual Inspection of Structures.” Journal of The Society of Naval Architects of Japan, Vol. 168, pp. 487-495.

10. Glisic, B. (2011). “Influence of gauge length to accuracy of long-gauge sensors employed in monitoring of prismatic beams,” Measurement Science and Technology, 22 (3), art. no. 035206 (13pp).